Journal of Photochemistry and Photobiology A: Chemistry 219 (2011) 132–138

Contents lists available at ScienceDirect

Journal of Photochemistry and Photobiology A: Chemistry

journal homepage: www.elsevier.com/locate/jphotochem

Synthesis and visible light photo-electrochemical behaviors of In_2O_3-sensitized ZnO nanowire array film

Fengling Zhou, Xinjun Li*, Jie Shu, Jing Wang

Key Laboratory of Renewable Energy and Gas Hydrate, Guangzhou Institute of Energy Conversion, Chinese Academy of Sciences, Guangzhou 510640, China

ARTICLE INFO

Article history:
Received 16 September 2010
Received in revised form
17 December 2010
Accepted 1 February 2011
Available online 1 March 2011

Keywords:
Photo-electrochemical behavior
In_2O_3
ZnO nanowire array
Carrier separation efficiency
Visible light

ABSTRACT

In_2O_3-sensitized ZnO nanowire (NW) array film with improving visible light activity was synthesized on F-doped SnO_2 (FTO) glass substrate by a facile two-step process. The films, ZnO NW arrays and In_2O_3-sensitized ZnO NW arrays, were characterized by X-ray diffraction (XRD), scanning electron microscopy (SEM) and UV–vis diffuse reflectance spectroscopy. For the films severed as the photoanodes in a three-electrode system, the photo-electrochemical behaviors were investigated and the photocatalytic activity was evaluated by the oxidation of glucose under visible light irradiation. The results show that the ZnO NW arrays are highly ZnO (0 0 2) orientated with a diameter of 100 nm and a length of 3 μm, and In_2O_3 nanoparticles grow and form a shell film on the wall of the ZnO NW array in the In_2O_3-sensitized ZnO NW array film. This composite structure shows a red shift from ultraviolet (λ = 385 nm) to the visible-light region (λ = 450 nm) in the maximum optical response. The incorporation of In_2O_3 into the ZnO NW array film remarkably promotes the photogenerated carrier separation and increases the utilization of photogenerated carriers in photocatalytic reactions, resulting in the higher photocatalytic activity under visible light.

1. Introduction

Since Fujishima and Honda discovered the photocatalytic splitting of water on a TiO_2 electrode under ultraviolet light in 1972 [1], semiconductor photocatalysts such as TiO_2 and ZnO have attracted tremendous attention from scientists and engineers [2,3]. In particular, zinc oxide (ZnO) [4] with a direct band gap of 3.2 eV films has been considered as one of the promising materials in the fields of hydrogen generation [5] and photocatalytic degradation for organic pollutants [6–8] under UV light irradiation.

Recently, many investigations have focused on preparing photocatalysts which can be activated by visible light [9] since there is much more energy produced by the sunlight in the visible lights region compared to the UV region [10]. One of the approaches to improve visible photocatalytic activity is to introduce the composite system by incorporating a narrow band gap semiconductor serving as the sensitizer to absorb visible light [11]. The narrow band gap semiconductors alone usually exhibit poor photocatalytic activity due to the recombination of photogenerated electron–hole pairs though it exhibits excellent response to visible light [12]. By introducing the composite system, it has demonstrated a high efficiency photocatalyst working under visible light [13] because it can compensate for the disadvantages of the individual component [5], and induce a synergistic effect, such as an efficient charge separation and improvement of photo stability. Several systems have been reported, e.g., ZnO/CdS [14], TiO_2/PbS [15], TiO_2/CdTe [16], and BiOCl/Bi_2O_3 [17], and proven to be efficient in photocatalysis.

Among a variety of semiconductor sensitizers, indium oxide (In_2O_3) with a band gap of 2.8 eV and a higher conduction band than that of ZnO [18,19] can be one of the ideal sensitizers used for ZnO because of the ideal position of its conduction and valence band edges [19]. Furthermore, an oxide shell can suppress the carrier's recombination by introducing an energy barrier and subsequently facilitate its separation [20]. And ZnO/In_2O_3 heteronanostructures nanoparticles have been proven a good performance in charge separation efficiency and photocatalytic activity [21,22].

However, up to date, there has been no report on the synthesis and photo-electrochemical behaviors of In_2O_3-sensitized ZnO nanowire (NW) array films. It is well-known that ZnO [4] NW film has demonstrated outstanding performance in the fields such as in dye sensitized solar cells [23,24] and photocatalytic degradation [25]. In contrast to common nanoparticle powders, this 1-dimension structure possesses larger surface areas [26], availability of low temperature synthesis, and potential for controlling the morphology through simple processing from solution [27], and higher charge-collection efficiencies [28]. The combination of In_2O_3 with ZnO NW could effectively overcome the narrow absorption range, and increase the charge separation efficiency [19], which

* Corresponding author. Tel.: +86 20 8705 7781; fax: +86 20 8705 7677.
E-mail address: lixj@ms.giec.ac.cn (X. Li).

1010-6030/$ – see front matter © 2011 Elsevier B.V. All rights reserved.
doi:10.1016/j.jphotochem.2011.02.002

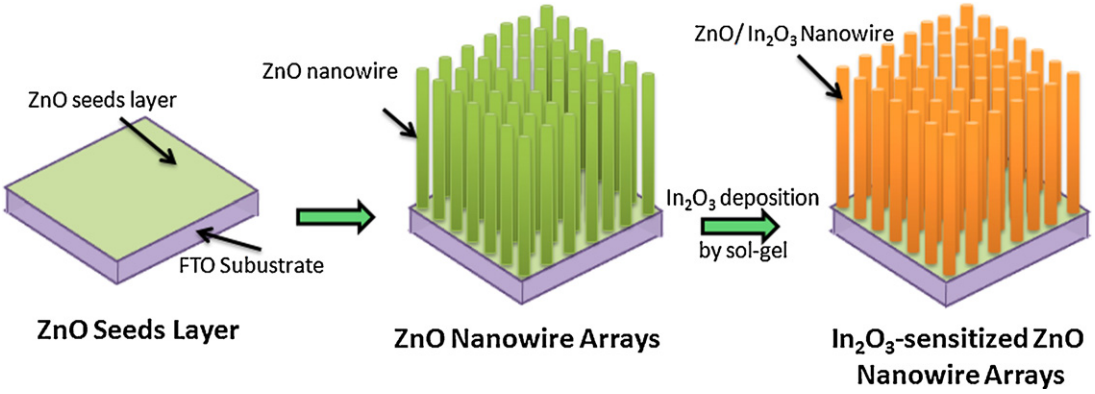

Fig. 1. Schematic showing the fabricating of In_2O_3-sensitized ZnO NW array film on FTO.

makes it a promising structure for the enhancement of the visible light assisted photo-electrochemical behaviors.

In this work, In_2O_3-sensitized ZnO NW array films were synthesized by incorporating the In_2O_3 onto the ZnO NW array film via dip-coating method using indium (III) chloride hydrate as the precursor. The effects of In_2O_3 on characteristics of the ZnO NW array films were investigated by comparing the photo-electrochemical behaviors of the ZnO NW array and In_2O_3-sensitized ZnO NW array electrodes in the three-electrode system.

2. Experiment

2.1. Material synthesis

All chemicals were used in the as-received condition without any further purification. The synthesis of the In_2O_3-sensitized ZnO NW array film was carried out by a two-step process: synthesis of ZnO NW arrays and sol–gel deposition of In_2O_3. The schematic fabricating of In_2O_3-sensitized ZnO NW array film is shown in Fig. 1 and the following is the details.

Step I: Synthesis of ZnO NW films. A typical procedure for synthesizing the ZnO NW films is carried out as in the literature [29]. Firstly, a seed layer was deposited on the conductive F-doped SnO_2 (FTO) glass by sol–gel method using the zinc acetate dihydrate ($Zn(Ac)_2{\cdot}2H_2O$, 0.5 mol L^{-1}) as the precursor and then the substrates coated with ZnO seed layer were calcined at 500 °C for 1 h. The precursor aqueous solution for the growth of ZnO NW was prepared in advance by mixing the hexamethylenetetramine (HMT, 0.025 mol L^{-1}) and $Zn(Ac)_2{\cdot}2H_2O$ (0.025 mol L^{-1}) in deionized water, and stirring for 20 min at 0 °C. Then the FTO substrates with ZnO seed layer were immersed into this solution immediately and sealed in a flask in an oven at 95 °C for 7 h. Then the films were rinsed in deionized water thoroughly and subsequently heated at 500 °C for 1 h. The film obtained in this step was marked as **ZNW**

Step II: Depositing of In_2O_3 on ZnO nanowire array films. The precursor solution for the deposition of In_2O_3 was prepared as follows: 0.01 mol of indium (III) chloride hydrate ($InCl_3{\cdot}5H_2O$) was mixed with 2 ml acetylacetone in 50 ml ethanol for 30 min, and then 1.5 ml ammonium hydroxide solution (25%) was added to form $In(OH)_3$. Then the as-prepared sol was deposited onto the obtained ZnO NW by dip-coating process, and subsequently the films were heated at 500 °C for 1 h. The amount of the incorporated In_2O_3 was controlled by the number of the cycles of dip-coating process, and the films obtained in this step with 5 and 10 times of dip-coating process were marked as **ZNWI-5** and **ZNWI-10**, respectively. In order to clarify the effect of ZnO NW in the system, In_2O_3 coated FTO electrodes without ZnO NW were prepared by comparable condition of ZNWI-5 and ZNWI-10, which were marked as **In-5** and **In-10**, respectively

2.2. Material characterization

The X-ray diffraction (XRD) experiments were carried out with a PANalytical XRD measurement, using Cu K_α radiation ($\lambda = 1.540598$ Å). The diffraction pattern was scanned in steps of 0.0170° (2θ) between 20° and 80°. The morphologies were characterized using a field-emission electron scanning microscopy (FESEM: Hitachi S-4300, Japan) equipped with an energy-dispersive X-ray analyzer (EDX: EDAX Genesis-60, America). A UV–vis spectrophotometer (U-3010) was employed to obtain the diffuse reflectance spectra of the samples.

2.3. Characterization of photo-electrochemical and photocatalytic activity

In order to investigate the photoelectrochemical behaviors of the films, photocurrent (i_{ph}), linear sweep voltammetry(LSV) and electrochemical impedance spectroscopy (EIS) were employed and all performed in the three-electrode system which was made of quartz cells linked with CHI660A electrochemical station (CH Instruments, USA) in 100 ml aqueous solution (containing 0.1 mol L^{-1} Na_2SO_4 + 0.4 mmol L^{-1} $K_4Fe(CN)_6$ + 0.4 mmol L^{-1} $K_3Fe(CN)_6$)[30,31]. The In_2O_3-sensitized ZnO NW arrays films, a Pt electrode, and a saturation calomel electrode served as working electrode, counter electrode and reference electrode, respectively. The working electrode surface area exposed to electrolyte was confined by an electrode holder with an opening area of 5 mm^2.

The photocatalytic activity was evaluated through the photo-electrochemical oxidation of glucose by using the films as the photoanodes in the three electrode system. A 100 ml aqueous solution containing 0.1 mol L^{-1} $NaNO_3$ was employed as a supporting electrolyte and the concentrations of glucose were adjusted in situ by carefully injecting the calculated amount of glucose solution into the reaction media.

All the photo-electrochemical tests were implemented under the illumination of a 300 W xenon lamp (with a visible band pass filter glass, 390–770 nm) at room temperature.

3. Result and discussion

3.1. Morphologies and structures

Fig. 2 gives XRD patterns of the FTO, ZnO NW and In_2O_3-sensitized ZnO NW arrays obtained. From Fig. 2, it is observed that (0 0 2) peak of ZnO is the strongest among all the peaks, showing

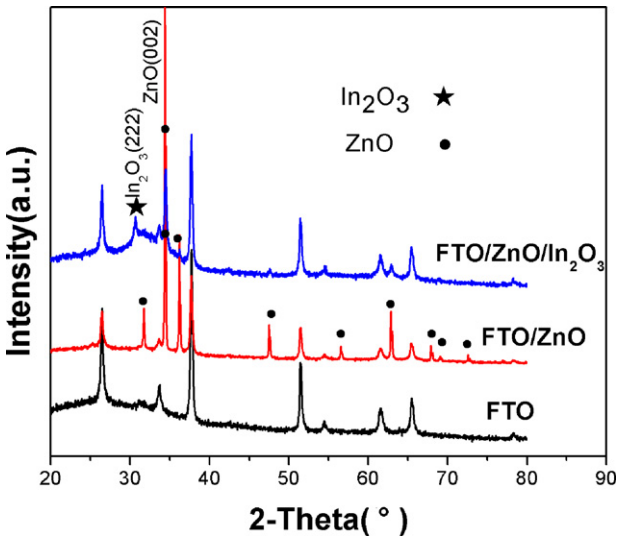

Fig. 2. XRD patterns of FTO, ZnO and In_2O_3-sensitized ZnO NW arrays.

that the ZnO nanowire arrays is preferentially oriented along the c-axis direction, and the peak of In_2O_3 (2 2 2) emerges after 10 cycles of dip-coating in indium (III) sol–gel.

In order to observe the surface morphology of the film, the surface and section morphologies of the FESEM images of the ZnO and In_2O_3-sensitized ZnO NW arrays are shown in Fig. 3. The morphology of the In_2O_3-sensitized ZnO NW could be controlled by experimental parameters such as the number of the cycles of dip-coating process of In_2O_3 sol (see in Section 2).

It can be observed that the ZnO film (Fig. 3a) is consisted of bare ZnO nanowire arrays with smooth walls (Fig. 3d and g) and a diameter of 100 nm, and the hexagon can be obviously found at the top of ZnO nanowire (Fig. 3d insert), which indicates a preferentially orientation along the c-axis direction. The cross-section image shows that the nanowire array is about 3 μm long (Fig. 3a insert). From the images, we could notice that the wall of the ZNWI-5 (Fig. 3e and h) is coarser than that of ZNW (Fig. 3d and g), and it also shows that the element of indium (In) emerges in the energy-dispersive X-ray (EDX) analysis (Fig. 3i), which indicates that In_2O_3 nanoparticles have grown and eventually coalesced to form a shell film on the wall of the ZnO nanowire array (Fig. 3e and h) after dip-coating process. While the morphology of ZnO nanowire arrays is still completely maintained, indicating that the excellent properties of ZnO nanowire do not change before and after In_2O_3 loading (Fig. 3b and e). However, ZnO nanowire arrays are almost covered by the In_2O_3 and the morphology is deteriorated when more In_2O_3 are deposited on the films (Fig. 3c and f).

3.2. UV–vis reflectivity spectra

It is important to study the optical absorption of the In_2O_3-sensitized ZnO NW array film because the UV–vis absorption edge is relevant to the energy band of semiconductor catalyst. And the diffuse reflectance spectrum of the ZnO and In_2O_3-sensitized ZnO

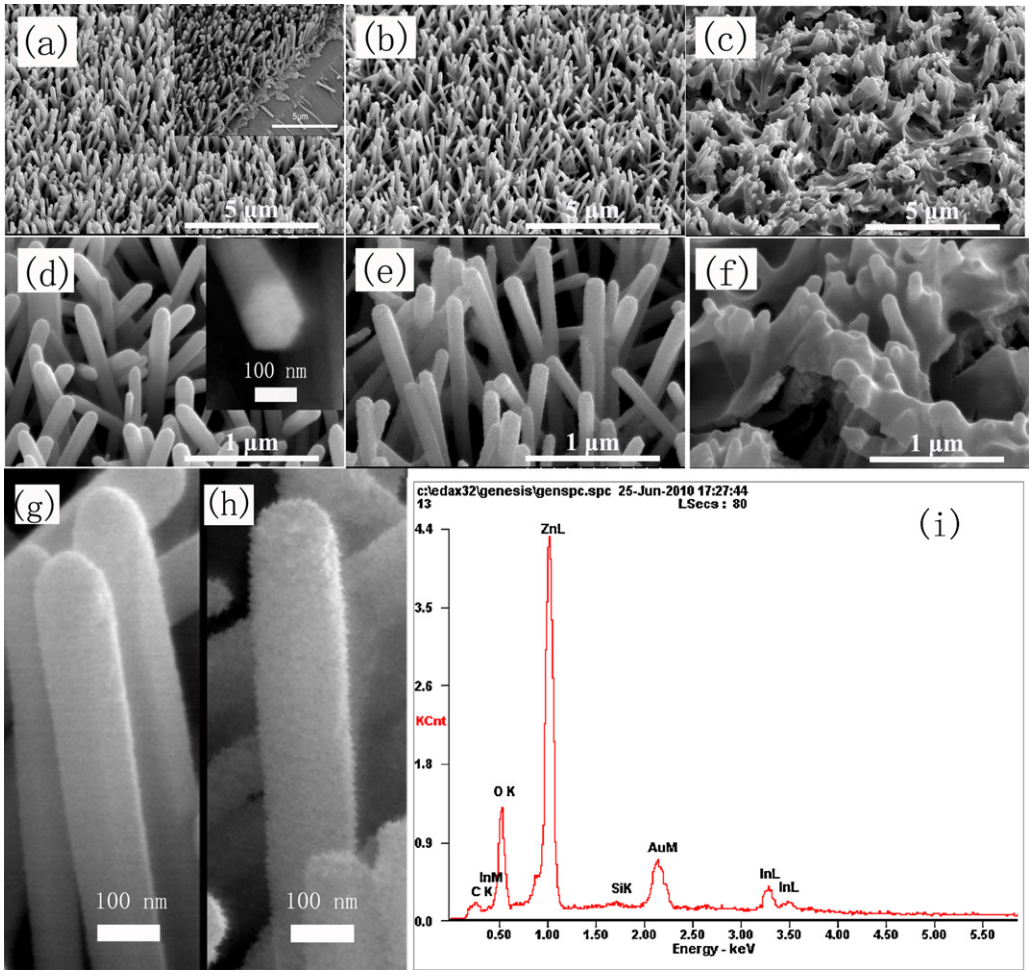

Fig. 3. FESEM images of ZnO and In_2O_3-sensitized ZnO NW arrays: (a, d, and g) ZNW; (b, e, and h) ZNWI-5; (c and f) ZNWI-10 and EDX analysis of ZNWI-5 (i).

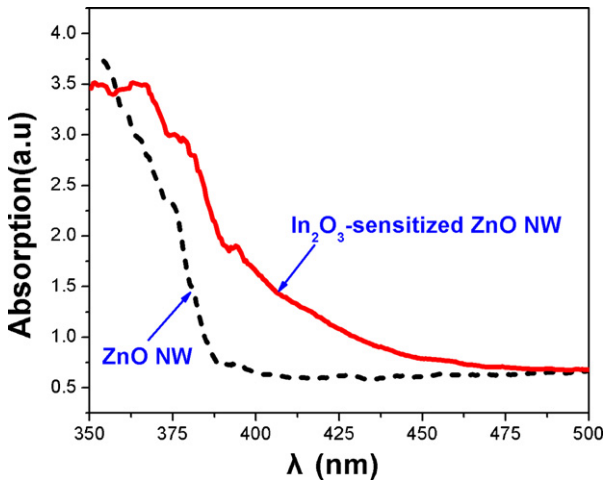

Fig. 4. UV–vis diffuse reflectance spectrum of the ZnO and In_2O_3-sensitized ZnO NW array films.

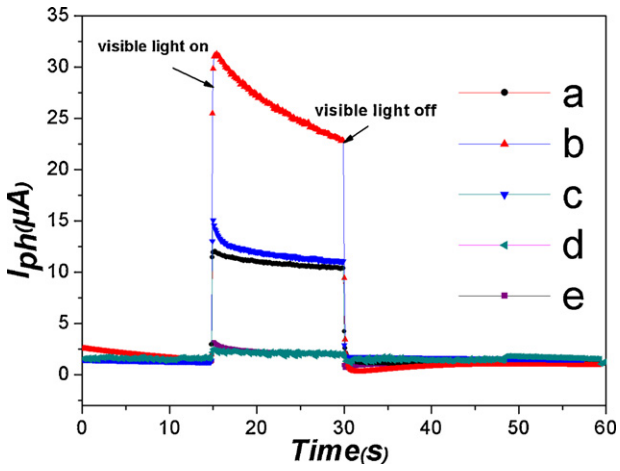

Fig. 5. Photocurrent of ZnO and In_2O_3-sensitized ZnO NW array films under visible illumination: (a) ZNW; (b) ZNWI-5; (c) ZNWI-10; (d) In-5; (e) In-10. Testing solution: 0.1 mol L^{-1} Na_2SO_4 + 0.4 mmol L^{-1} $K_4Fe(CN)_6$ + 0.4 mmol L^{-1} $K_3Fe(CN)_6$.

NW array films in the wavelength region between 350 and 600 nm is shown in Fig. 4.

It can be seen from Fig. 4 that the ZnO nanowire array film shows an absorption edge at 385 nm which is in accordance with that of bulk ZnO. When the film incorporated with In_2O_3, the absorption edge moves towards larger wavelength at 450 nm shown in the absorption spectrum, which is accordance with the absorption edge of In_2O_3. The red shift indicates that the film incorporated with In_2O_3 has an effective absorption of visible light, resulting in an activity for visible light in the In_2O_3-sensitized ZnO NW film.

3.3. The characterization of photo-electrochemical behaviors and photocatalytic activity

When semi-conductive materials are illuminated with light, the photoelectrons would be excited from the valance band to the conducting band and then transient photocurrent (i_{ph}) is generated. There is a linear relationship between the value of the transient photocurrent and the conductance value which indicates the number of free current carriers in the semiconductor. And it is well established that LSV can be used to investigate the redox performance of semi-conductive films [32]. The photocurrent increased linearly with the applied potential could represent the photocatalytic oxidation of semi-conductive films by photoholes at the interface [33]. Electrochemical method is usually used to characterize charge separation of the films [34,35]. The separation efficiency of the photogenerated electron–hole pairs and charge transfer resistance are always evaluated by EIS plots. The charge-transfer rate constant (k_{ctrc}) can be calculated from EIS Bode graph ($k_{ctrc} = \omega_{max}$) [35]. And a larger curvature radius in Nyquist usually denotes a larger charge transfer resistance and a lower separation efficiency of the photogenerated electron–hole pairs [34].

Herein, i_{ph}, LSV and EIS were chosen to estimate the photogenerated carriers' separation performance of the films serving as photoanodes in the three-electrode system under visible illumination.

3.3.1. Photo-electrochemical behaviors

Fig. 5 shows i_{ph} of In_2O_3, ZnO and In_2O_3-sensitized ZnO NW array films measured under visible illumination in the electrolyte (containing 0.1 mol L^{-1} Na_2SO_4 + 0.4 mmol L^{-1} $K_4Fe(CN)_6$ + 0.4 mmol L^{-1} $K_3Fe(CN)_6$) at the constant potential bias of 0.5 V. The i_{ph} of In_2O_3-sensitized ZnO NW array film is remarkably enhanced compared with that of ZnO nanowire array film (Fig. 5a) or In_2O_3 films (Fig. 5d and e) under visible illumination. It indicates that there are a larger number of free photogenerated carriers in ZNWI-5 (Fig. 5b) than that in ZnO nanowire array film (Fig. 5a) or In_2O_3 films (Fig. 5d and e) under visible illumination. However, it also shows that when more In_2O_3 nanoparticles are deposited on the ZnO nanowire arrays, there is a decrease of i_{ph} under visible illumination (Fig. 5c), which indicates that more amount of incorporated In_2O_3 particles deteriorates the photo-electrochemical property of the films.

LSV voltammograms of ZnO and In_2O_3-sensitized ZnO NW array films measured in dark and under visible illumination in the electrolyte (containing 0.1 mol L^{-1} Na_2SO_4 + 0.4 mmol L^{-1} $K_4Fe(CN)_6$ + 0.4 mmol L^{-1} $K_3Fe(CN)_6$) at a scan rate of 5 mV/s from 1 V to −1 V are shown in Fig. 6. It is clearly seen that the anodic photocurrent of In_2O_3-sensitized ZnO NW array film (Fig. 6b) is much higher than that of ZnO nanowire array film (Fig. 6a) under visible illumination which reveals that there are a larger number of free photogenerated carriers in In_2O_3-sensitized ZnO NW array films [34]. Here the anodic photocurrent represents photocatalytic oxidation of water by photoholes in films which explicates that there are more photoholes in In_2O_3-sensitized ZnO NW array films [34]. Furthermore, both the ZnO NW and In_2O_3-sensitized ZnO NW array film show a sharp increase at the catholic currents with the increase of the negative potential, and they exhibit negative photo-potential

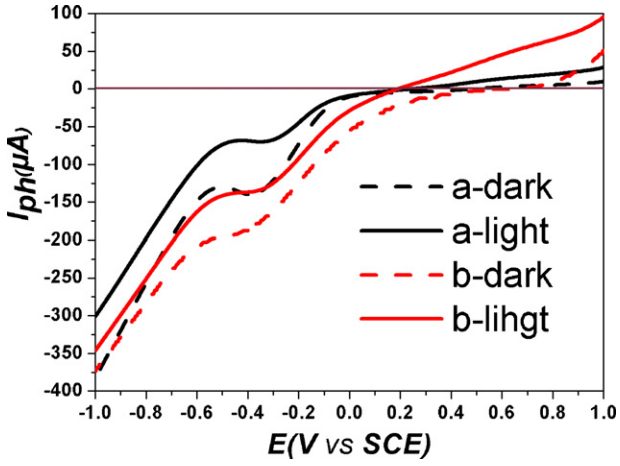

Fig. 6. LSV Plots of the ZnO and In_2O_3-sensitized ZnO NW array films under visible illumination: (a) ZNW; (b) ZNWI-5. Testing solution: 0.1 mol L^{-1} Na_2SO_4 + 0.4 mmol L^{-1} $K_4Fe(CN)_6$ + 0.4 mmol L^{-1} $K_3Fe(CN)_6$.

Table 1
Parameters obtained by fitting the impedance spectra of ZnO and In_2O_3-sensitized ZnO NW films.

Electrodes	R_{ctr} (Ω)	$k_{ctr} = \omega_{max}$ (s^{-1})
ZNW	47400	1.41
ZNWI-5	19083	3.23
ZNWI-10	34455	1.41

under visible illumination by comparing with the situation in dark (Fig. 6), indicating an n-type semiconductor behavior [30,31].

Fig. 7 presents the EIS spectra (Bode and Nyquist) of the ZnO and In_2O_3-sensitized ZnO NW array electrodes under visible illumination in the electrolyte (containing 0.1 mol L^{-1} Na_2SO_4 + 0.4 mmol L^{-1} $K_4Fe(CN)_6$ + 0.4 mmol L^{-1} $K_3Fe(CN)_6$).The frequencies for EIS measurement were set from 10^5 to 0.01 Hz. The parameters of the charge transfer rate constant (k_{ctrc}) and charge transport resistance (R_{ctr}) obtained by fitting the impendence spectra [35] are shown in Table 1. As shown in Fig. 7, the circular radius and calculated R_{ctr} of ZNWI-5 electrode are dramatically smaller than that of ZNW arrays electrode, indicating that the ZNWI-5 electrode has lower charge transport resistance than the ZnO NW arrays electrode. Moreover, the result of calculated k_{ctrc} in Table 1 obtained by EIS Bode shows that ZNWI-5 has a larger charge transfer rate constant (3.23 s^{-1}) compared with ZnO NW (1.41 s^{-1}), which mean higher separation efficiency of the photoelectrons and photoholes in ZNWI-5. It could be explained that the recombination of photogenerated electron–hole pairs is effectively inhibited by the incorporation of In_2O_3, resulting in better charge separation in the films. Thus, the photocurrents of ZNWI nanowire array films are also evidently improved under visible light (Fig. 5).

Furthermore, Fig. 7 also shows that the circular radius of ZNWI-10 electrode (Fig. 7c) is larger than that of ZNWI-5 electrode, which means a higher charge transport resistance in ZNWI-10, which may be responsible for the reduce of the photocurrent in this film (Fig. 5).

3.3.2. *Photoelectrochemical oxidation of glucose*

To evaluate the effect of incorporated In_2O_3 on the photo-electrocatalytic activity of the ZnO nanowire arrays, we studied the photo-electrochemical oxidation of glucose by using the films as the photoanodes in the three electrode system which was made of quartz cells linked with CHI660A electrochemical station.

Photoelectrochemical oxidation of glucose is considered to be an effective method to evaluate the photo-catalytic activity of semiconductor film, and the principle and calculation have been well illustrated in Zhang's work [2,36] and our previous research [37].

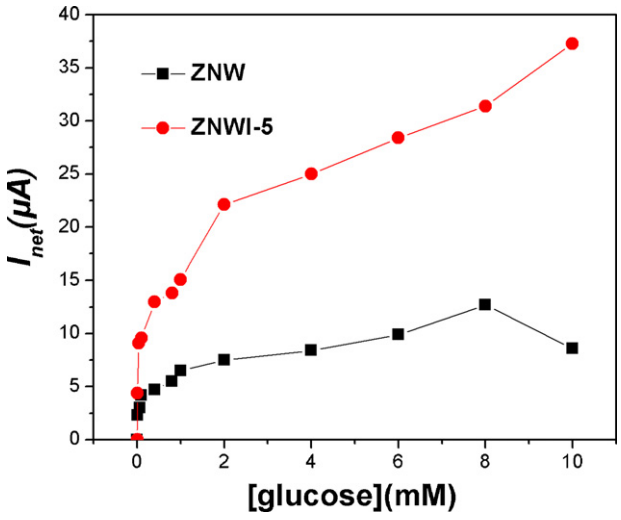

Fig. 8. i_{net} plots vs concentration of glucose of ZNW andZNWI-5 films under visible illumination. Supporting electrolyte: 0.1 mol L^{-1} $NaNO_3$.

And, the photocurrent obtained in the organic compounds oxidation directly represents the photo-electrocatalytic activity and effectiveness of oxidation process. The photocurrent coming from the oxidation of organic species (i_{net}) can be calculated by subtracting photocurrent coming from the oxidation of water (i_{blank}) in electrolyte without organic compounds from the overall photocurrent measured in the experiment (i_{ph}) in electrolyte with organic compounds according Eq. (1). For given experimental conditions, i_{net} can be used to represent the oxidation rate of the organic species and therefore the photoelectrocatalytic efficiency of the electrode.

$$i_{net} = i_{ph} - i_{blank} \quad (1)$$

The photo-electrochemical oxidation of glucose on ZNW and ZNWI-5 electrodes were investigated at the constant potential bias of 0.8 V. And the functions of the i_{net} vs glucose concentration for ZNW and ZNWI-5 nanowire array films under visible illumination are shown in Fig. 8.

The results show that, for both tested electrodes, the i_{net} increased with the increasing glucose concentration. What is more, the ZNWI-5 electrode possessed higher i_{net} value under visible illumination (Fig. 8b), compared with the ZNW electrode. This suggests that the photoelectrocatalytic reaction of glucose on the surface of ZNWI-5 electrode is faster than that on the surface of ZNW electrode. In other words, the ZNWI-5 electrode has a higher pho-

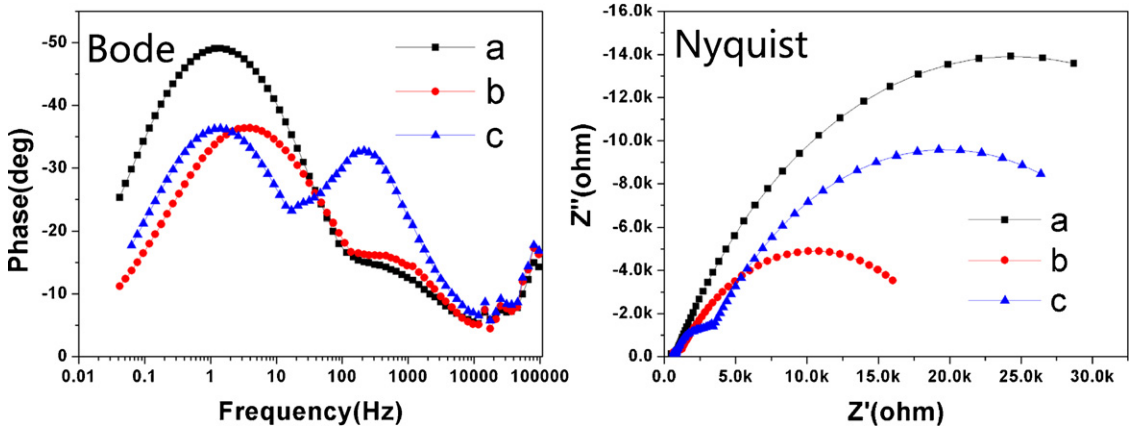

Fig. 7. EIS plots (Bode and Nyquist) of ZnO and In_2O_3-sensitized ZnO NW films under visible illumination: (a) Z NW; (b) ZNWI-5; (c) ZNWI-10. Testing solution: 0.1 mol L^{-1} Na_2SO_4 + 0.4 mmol L^{-1} $K_4Fe(CN)_6$ + 0.4 mmol L^{-1} $K_3Fe(CN)_6$.

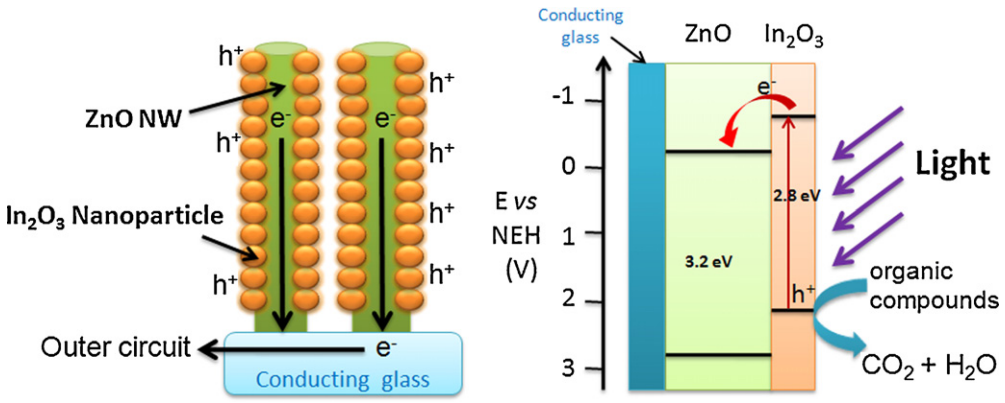

Fig. 9. Schematic showing the mechanism of the enhancement of photo-electrochemical behaviors of In_2O_3-sensitized ZnO NW array films.

toelectrocatalytic activity for glucose than ZnO nanowire electrode under visible illumination (Fig. 8), which is consistent with the aforementioned results obtained from i_{ph}, LSV and EIS measurement (Figs. 5–7).

3.4. Mechanism discussion

Fig. 9 shows the supposed schematic mechanism of the enhancement of photo-electrochemical behaviors of In_2O_3-sensitized ZnO NW array film. The In_2O_3 has a 2.8 eV [38] band gap with a conducting band at −0.62 (E vs NEH) and valance band at 2.18 (E vs NEH), while ZnO has a 3.2 eV band gap with a conducting band at −0.31 (E vs NEH) and valance band at 2.89 (E vs NEH) [39].

When In_2O_3 is illuminated by visible light, the photoelectrons would be excited from the valance band to the conducting band and then transient photocurrent is generated. However, in most instances, the valence band holes and conduction band electrons simply recombine liberating heat or light, a process known as recombination, which is responsible for the low photon conversion efficiency [11,40] (Fig. 5d and e). Thus, the inhibition of the recombination and enhancement of separation efficiency of photogenerated electron–hole pairs are quite important for the improvement of the photo-electrochemical behaviors [21].

We suppose that the enhancement of the photo-electrochemical property of the In_2O_3-sensitized ZnO nanowire array film may be contributed by the coupling effects of ZnO NW arrays and In_2O_3 shells as a kind of heterostructure [14,19]. On one hand, the incorporation of In_2O_3 introduces a certain amount of visible light-sensitive nanoparticles coating on the wall of ZnO nanowire arrays. Once visible light excitation occurs, the In_2O_3 coating itself effectively absorbs light and produces photoelectrons and then the photoelectrons are injected to the lower ZnO conducting band [14,22], leaving photoholes on the surfaces to participate the photo-electrochemical reaction. And thus, the rate of hole–electron recombination in In_2O_3 is suppressed, which effectively improves the carrier separation efficiency. The photogenerated holes transfer to the surface of In_2O_3 rather than undergoing bulk recombination, and then would be effectively scavenged by the water or glucose, and as a result it enhances the photo-electrochemical behaviors directly. In the mean time, thanks to the high electron mobility and the geometry of the vertical-aligned ZnO nanowire arrays, the injected electrons are effectively collected due to the remarkably reduce of the electrons transport distance in the photo-anode, which promotes the photo-electrochemical behaviors indirectly. Therefore, the incorporation of In_2O_3 highly enhances the photo-electrochemical behaviors of In_2O_3-sensitized ZnO NW array films (Figs. 5–7), and the photogenerated holes have more opportunity to participate in the photoelectrocatalytic oxidation reaction (Fig. 8). Thus, we suppose that the coupling effect between the structures and electronic configurations of ZnO and In_2O_3 is mainly responsible for the high photoelectrocatalytic activity of In_2O_3-sensitized ZnO NW array films.

Besides, as larger amount of incorporated In_2O_3 nanoparticles increase the thickness of the In_2O_3 shell (Fig. 3c and f) and introduce a larger number of grain boundaries, and thus, the photogenerated electrons in In_2O_3 have to transfer a longer distance to the ZnO NW arrays, resulting the increase of the charge transfer resistance (Fig. 7c) and lower carrier separation efficiency. Hence, the larger amount of incorporated In_2O_3 does not improve the photo-electrochemical behaviors of films, but instead, decrease the photo-electrochemical properties (Figs. 5c and 7c).

4. Conclusion

In summary, In_2O_3-sensitized ZnO nanowire array film has been successfully synthesized on FTO glasses by a facile two-step process. XRD and SEM results show that In_2O_3 nanoparticles grow and form a shell film on the wall of the ZnO nanowire array in the In_2O_3-sensitized ZnO NW array film. Optical spectra indicates that In_2O_3-sensitized ZnO NW array film shows effective absorption of visible light with an absorption edge at 450 nm. And the results of the photo-electrochemical behavior characterization under visible light show that the i_{ph}, and carrier separation efficiency are remarkably improved in the In_2O_3-sensitized ZnO NW array films compared with that of ZnO nanowire array films. Besides, the In_2O_3-sensitized ZnO NW electrode possesses higher i_{net} values in the photo-electrochemical oxidation of glucose than that of ZnO nanowire array films which indicates a remarkable enhancement of photoelectrocatalytic activity for glucose in the In_2O_3-sensitized ZnO NW array films under visible illumination. Furthermore, the mechanism for this enhancement is proposed, and it may be contributed by the coupling effects of ZnO NW arrays and In_2O_3 shells, resulting the improved photo-electrochemical behavior and photocatalytic activity under visible illumination.

Acknowledgement

The work was financially supported by the Guangdong Province and Ministry of Education of China (No. 2008A090400011), Guangdong key Laboratory of Clean Energy Technology (No. 2008A060301002), Knowledge Innovation Program of the Chinese Academy of Sciences (No. KGCX2-YW-343) and National 973 project of China (No. 2009CB220002).

References

[1] Fujishima, K. Honda, Electrochemical photolysis of water at a semiconductor electrode, Nature 238 (1972) 37–38.
[2] M. Yang, L.H. Li, S.Q. Zhang, G.Y. Li, H.J. Zhao, Preparation, characterisation and sensing application of inkjet-printed nanostructured TiO_2 photoanode, Sens. Actuators B 147 (2010) 622–628.
[3] M. Janus, J. Choina, A.W. Morawski, Azo dyes decomposition on new nitrogen-modified anatase TiO_2 with high adsorptivity, J. Hazard. Mater. 166 (2009) 1–5.
[4] P.H. Yeh, Z. Li, Z.L. Wang, Schottky-gated probe-free ZnO nanowire biosensor, Adv. Mater. 21 (2009) 4975–4978.
[5] G.M. Wang, X.Y. Yang, F. Qian, J.Z. Zhang, Y. Li, Double-sided CdS and CdSe quantum dot co-sensitized ZnO nanowire arrays for photoelectrochemical hydrogen generation, Nano Lett. 10 (2010) 1088–1092.
[6] N.K. Allam, K. Shankar, C.A. Grimes, Photoelectrochemical and water photoelectrolysis properties of ordered TiO_2 nanotubes fabricated by Ti anodization in fluoride-free HCl electrolytes, J. Mater. Chem. 18 (2008) 2341–2348.
[7] G. Tanarungsun, W. Kiatkittipong, P. Praserthdam, H. Yamada, T. Tagawa, S. Assabumrungrat, Hydroxylation of benzene to phenol on Fe/TiO_2 catalysts loaded with different types of second metal, Catal. Commun. 9 (2008) 1886–1890.
[8] S.S. Soni, M.J. Henderson, J.F. Bardeau, A. Gibaud, TiO_2 nanoparticles with high photocatalytic activity under visible light, Adv. Mater. 20 (2008) 1493–1498.
[9] M. Janus, B. Tryba, E. Kusiak, T. Tsumura, M. Toyoda, M. Inagaki, A.W. Morawski, TiO_2 nanoparticles with high photocatalytic activity under visible light, Catal. Lett. 128 (2009) 36–39.
[10] M. Asilturk, F. Sayilkan, E. Arpac, Effect of Fe^{3+} ion doping to TiO_2 on the photocatalytic degradation of malachite green dye under UV and vis-irradiation, J. Photochem. Photobiol., A 203 (2009) 64–71.
[11] A.W. Morawski, M. Janus, B. Tryba, M. Toyoda, T. Tsumura, M. Inagaki, Carbon modified TiO_2 photocatalysts for water purification, Pol. J. Chem. Technol. 11 (2009) 46–50.
[12] T.J. Yan, J.L. Long, X.C. Shi, D.H. Wang, Z.H. Li, X.X. Wang, Efficient photocatalytic degradation of volatile organic compounds by porous indium hydroxide nanocrystals, Environ. Sci. Technol. 44 (2010) 1380–1385.
[13] X.W. Zuo, F. Peng, C.L. Hu, B.T. Su, Z.Q. Lei, Preparation of magnetic TiO_2/$CoFe_2O_4$ composite photocatalytic nanomaterial, Chin. J. Inorg. Chem. 25 (2009) 1233–1237.
[14] Y. Tak, H. Kim, D. Lee, K. Yong, Type-II CdS nanoparticle-ZnO nanowire heterostructure arrays fabricated by a solution process: enhanced photocatalytic activity, Chem. Commun. (2008) 4585–4587.
[15] R. Brahimi, Y. Bessekhouad, A. Bouguelia, M. Trari, Improvement of eosin visible light degradation using PbS-sensititized TiO_2, J. Photochem. Photobiol., A 194 (2008) 173–180.
[16] X.F. Gao, H.B. Li, W.T. Sun, Q. Chen, F.Q. Tang, L.M. Peng, CdTe quantum dots-sensitized TiO_2 nanotube array photoelectrodes, J. Phys. Chem. C 113 (2009) 7531–7535.
[17] S.Y. Chai, Y.J. Kim, M.H. Jung, A.K. Chakraborty, D. Jung, W.I. Lee, Heterojunctioned BiOCl/Bi_2O_3, a new visible light photocatalyst, J. Catal. 262 (2009) 144–149.
[18] Yaglioglu, Y.J. Huang, H.Y. Yeom, D.C. Paine, A study of amorphous and crystalline phases in In_2O_3–10 wt.% ZnO thin films deposited by DC magnetron sputtering, Thin Solid Films 496 (2006) 89–94.
[19] I.G. Benjaram, M. Reddy, Ataullah Khan, Preparation and characterization of In_2O_3-TiO_2 and V_2O_5/In_2O_3-TiO_2 composite oxides for catalytic applications, Appl. Catal., A 248 (2003) 169–180.
[20] M. Law, L.E. Greene, A. Radenovic, T. Kuykendall, J. Liphardt, P.D. Yang, ZnO-Al_2O_3 and ZnO-TiO_2 core–shell nanowire dye-sensitized solar cells, J. Phys. Chem. B 110 (2006) 22652–22656.
[21] Z.Y. Wang, B.B. Huang, Y. Dai, X.Y. Qin, X.Y. Zhang, P. Wang, H.X. Liu, J.X. Yu, Highly photocatalytic ZnO/In_2O_3 heteronanostructures synthesized by a coprecipitation method, J. Phys. Chem. C 113 (2009) 4612–4617.
[22] Hotchandani, P.V. Kamat, Charge-transfer processes in coupled semiconductor systems—photochemistry and photoelectrochemistry of the colloidal Cds–ZnO system, J. Phys. Chem. 96 (1992) 6834–6839.
[23] S.H. Lee, S.H. Han, H.S. Jung, H. Shin, J. Lee, J.H. Noh, S. Lee, I.S. Cho, J.K. Lee, J. Kim, H. Shin, Al-doped ZnO thin film: a new transparent conducting layer for ZnO nanowire-based dye-sensitized solar cells, J. Phys. Chem. C 114 (2010) 7185–7189.
[24] J.J. Qiu, X.M. Li, F.W. Zhuge, X.Y. Gan, X.D. Gao, W.Z. He, S.J. Park, H.K. Kim, HwangF d Y.H., Solution-derived 40 μm vertically aligned ZnO nanowire arrays as photoelectrodes in dye-sensitized solar cells, Nanotechnology 21 (2010) 195602.
[25] J.L. Yang, S.J. An, W.I. Park, G.C. Yi, W. Choi, Photocatalysis using ZnO thin films and nanoneedles grown by metal–organic chemical vapor deposition, Adv. Mater. 16 (2004) 1661–1664.
[26] K. Zhu, N.R. Neale, A. Miedaner, A.J. Frank, Enhanced charge-collection efficiencies and light scattering in dye-sensitized solar cells using oriented TiO_2 nanotubes arrays, Nano Lett. 7 (2007) 69–74.
[27] J.B. Cui, Y.C. Soo, T.P. Chen, U.J. Gibson, Low-temperature growth and characterization of Cl-doped ZnO nanowire arrays, J. Phys. Chem. C 112 (2008) 4475–4479.
[28] P. Gao, Z.Z. Wang, K.H. Liu, Z. Xu, W.L. Wang, X.D. Bai, E.G. Wang, Photoconducting response on bending of individual ZnO nanowires, J. Mater. Chem. 19 (2009) 1002–1005.
[29] J.J. Qiu, W.D. Yu, X.D. Gao, X.M. Li, Sol–gel assisted ZnO nanorod array template to synthesize TiO_2 nanotube arrays, Nanotechnology 17 (2006) 4695–4698.
[30] K. Singh, S.S.D. Mishra, Photoelectrochemical studies on galvanostatically formed cadmium selenide films using mixed solvents, Sol. Energy Mater. Sol. Cells 63 (2000) 275–284.
[31] K. Singh, S.S.D. Mishra, Photoelectrochemical studies on galvanostatically formed multiple band gap materials based on CdSe and ZnSe, Sol. Energy Mater. Sol. Cells 71 (2002) 115–129.
[32] S.Q. Zhang, D.J. Jiang, H.J. Zhao, Development of chemical oxygen demand online monitoring system based on a photoelectrochemical degradation principle, Environ. Sci. Technol. 40 (2006) 2363–2368.
[33] D.Z. Jiang, H.J. Zhao, Z.B. Jia, J.L. Cao, R. John, Photoelectrochemical behaviour of methanol oxidation at nanoporous TiO_2 film electrodes, J. Photochem. Photobiol., A 144 (2001) 197–204.
[34] J. Zheng, H. Yu, X. Li, S. Zhang, Enhanced photocatalytic activity of TiO_2 nanostructured thin film with a silver hierarchical configuration, Appl. Surf. Sci. 254 (2008) 1630.
[35] W.H. Leng, Z. Zhang, J.Q. Zhang, C.N. Cao, Investigation of the kinetics of a TiO_2 photoelectrocatalytic reaction involving charge transfer and recombination through surface states by electrochemical impedance spectroscopy, J. Phys. Chem. B 109 (2005) 15008–15023.
[36] S.Q. Zhang, W. Wen, H.Z. Zhang, H.J. Zhao, In situ photoelectrochemical measurement of phthalic acid on titania, J. Photochem. Photobiol., A 208 (2009) 97–103.
[37] J. Wang, Y.H. Han, M.Z. Feng, J.Z. Chen, X.J. Li, S.Q. Zhang, Preparation and photoelectrochemical characterization of WO3/TiO2 nanotube array electrode, J. Mater. Sci. 46 (2011) 416–421.
[38] L.X. Zhang, Y.C. Zhang, M. Zhang, Synthesis and photoluminescence of In_2O_3 nanocrystals and submicron crystals from $InCl_3 \cdot 4H_2O$ and thiourea, Mater. Lett. 64 (2010) 966–968.
[39] X.D. Gao, X.M. Li, W.D. Yu, L. Li, J.J. Qiu, Seed layer-free synthesis and characterization of vertically grown ZnO nanorod array via the stepwise solution route, Appl. Surf. Sci. 253 (2007) 4060–4065.
[40] Y.S. Chen, J.C. Crittenden, S. Hackney, L. Sutter, D.W. Hand, Preparation of a novel TiO_2-based *p–n* junction nanotube photocatalyst, Environ. Sci. Technol. 39 (2005) 1201–1208.